The nucleoporin ALADIN regulates Aurora A localization to ensure robust mitotic spindle formation

Sara Carvalhal[a], Susana Abreu Ribeiro[b,c], Miguel Arocena[a,*], Taciana Kasciukovic[a], Achim Temme[d], Katrin Koehler[e], Angela Huebner[e], and Eric R. Griffis[a,b]

[a]Centre for Gene Regulation and Expression, University of Dundee, College of Life Sciences, Dundee DD1 5EH, United Kingdom; [b]Physiology Course, Marine Biological Laboratory, Woods Hole, MA 02543; [c]Wellcome Trust Centre for Cell Biology, Institute of Cell and Molecular Biology, University of Edinburgh, Edinburgh EH9 3JR, United Kingdom; [d]Department of Neurosurgery and [e]Department of Paediatrics, University Hospital Carl Gustav Carus, Technische Universität Dresden, D-01307 Dresden, Germany

ABSTRACT The formation of the mitotic spindle is a complex process that requires massive cellular reorganization. Regulation by mitotic kinases controls this entire process. One of these mitotic controllers is Aurora A kinase, which is itself highly regulated. In this study, we show that the nuclear pore protein ALADIN is a novel spatial regulator of Aurora A. Without ALADIN, Aurora A spreads from centrosomes onto spindle microtubules, which affects the distribution of a subset of microtubule regulators and slows spindle assembly and chromosome alignment. ALADIN interacts with inactive Aurora A and is recruited to the spindle pole after Aurora A inhibition. Of interest, mutations in ALADIN cause triple A syndrome. We find that some of the mitotic phenotypes that we observe after ALADIN depletion also occur in cells from triple A syndrome patients, which raises the possibility that mitotic errors may underlie part of the etiology of this syndrome.

INTRODUCTION

In higher eukaryotes, the transition from interphase to mitosis requires a rapid and complete reorganization of the microtubule cytoskeleton to form the mitotic spindle. The spindle is assembled by the concerted effort of centrosomes, microtubule nucleators, motor proteins, and cross-linkers and orchestrates the alignment of chromosomes from prophase through metaphase and then their segregation to daughter cells at anaphase. To regulate such a dramatic change in cellular activity, a suite of mitotic kinases regulates hundreds of different spindle substrates (Olsen *et al.*, 2010) to modify

their activities and localization. One of the most important of these regulators is the serine/threonine kinase Aurora A.

Aurora A resides at the centrosome and spindle pole and is essential for centrosome maturation, mitotic entry, spindle assembly, and anaphase microtubule function (Sardon *et al.*, 2010; Lioutas and Vernos, 2014). Aurora A catalytic activity depends on autophosphorylation on threonine 288 and its association with Tpx2 (Littlepage *et al.*, 2002; Bayliss *et al.*, 2003; Eyers and Maller, 2004; Dodson and Bayliss, 2012; Dodson *et al.*, 2013; Zorba *et al.*, 2014). Key cofactors such as Ajuba, Bora, PAK, protein phosphatase inhibitor-2, and nucleophosmin also contribute to regulating Aurora A's activity and/or localization, and protein phosphatase 6 serves to inactivate the enzyme (Hirota *et al.*, 2003; Satinover *et al.*, 2004; Zhao *et al.*, 2005; Hutterer *et al.*, 2006; Zeng *et al.*, 2010; Reboutier *et al.*, 2012). Inhibition of Aurora A activity results in catastrophic errors in spindle assembly and chromosome segregation (Asteriti *et al.*, 2014).

NuMA is one critical Aurora A substrate that is essential for building the mitotic spindle (Compton and Cleveland, 1993; Sardon *et al.*, 2010; Toughiri *et al.*, 2013). NuMA binds to microtubule minus ends and the minus end–directed motor protein complex dynein/dynactin and undergoes a dramatic relocalization during the cell cycle, moving from the interphase nucleus to spindle poles and the polar cell cortex in mitosis, where it is essential for focusing spindle poles and

anchoring cortical microtubules (Merdes et al., 1996, 2000; Bowman et al., 2006). Aurora A is essential for regulating the localization of NuMA. When NuMA cannot be phosphorylated by Aurora A, it does not localize as well to the interphase nucleus and is enriched on the cell cortex (Toughiri et al., 2013). In addition to being an Aurora A–regulated spindle assembly factor, NuMA is an example of a kind of protein seen in higher eukaryotes, proteins with roles in the interphase nucleus that take on unrelated roles during mitosis.

When the membranes of the nuclear envelope are either partially or totally fenestrated to allow for microtubules to capture duplicated and linked chromatids, many factors that are sequestered in the nucleus during interphase are released. In addition, the nuclear lamina and nuclear pore complexes are largely disassembled during mitosis, which has freed these proteins and nuclear transport factors to evolve secondary roles during mitosis to ensure the accurate transmission of genetic material to daughter cells (Chatel and Fahrenkrog, 2011).

The first evidence that nuclear pore proteins (Nups) could have roles in mitosis came from the observation that some of these proteins were associating with kinetochores during mitosis (Belgareh et al., 2001). Subsequent studies showed that several Nups and lamins are required for proper kinetochore and spindle function, spindle assembly checkpoint signaling, and nuclear envelope breakdown and reassembly (Arnaoutov and Dasso, 2003; Babu et al., 2003; Harel et al., 2003; Joseph et al., 2004; Loiodice et al., 2004; Blower et al., 2005; Jeganathan et al., 2005; Orjalo et al., 2006; Prunuske et al., 2006; Tsai et al., 2006; Lee et al., 2008; Rasala et al., 2008; Klein et al., 2009; Lince-Faria et al., 2009; Platani et al., 2009; Goodman et al., 2010; Mishra et al., 2010; Xu and Powers, 2010; Cross and Powers, 2011; Itoh et al., 2013). In addition, the Ran GTPase, which is a master regulator of nuclear transport, plays a crucial role in forming the mitotic spindle by regulating the association of transport proteins with spindle assembly factors (reviewed in Silverman-Gavrila and Wilde, 2006; Ciciarello et al., 2007; Kalab and Heald, 2008).

In addition to roles in transport and mitosis, Nups play important roles in genome architecture, cancer, transcription, and inherited diseases. For example, the nucleoporin ALADIN (the product of the AAAS gene) is mutated in patients who suffer from triple A (achalasia-Addisonianism-alacrima) or Allgrove syndrome, a disease that typically affects tear production, esophageal motility, and adrenal glucocorticoid and mineralocorticoid secretion in children (Handschug et al., 2001; Cronshaw et al., 2002). Many adult triple A patients suffer from progressive neurological features, including sensorimotor neurodegeneration, dysautonomia, optical atrophy, and ataxia. There is no consensus as to how mutations in ALADIN produce such variable phenotypes. Most ALADIN mutants fail to localize to the nuclear pore complex, and deficits in the nuclear import of DNA repair proteins and/or ferritin and the regulation of redox homeostasis have been proposed to play a role in the progressive degeneration seen in affected tissues (Cronshaw and Matunis, 2003; Hirano et al., 2006; Krumbholz et al., 2006; Storr et al., 2009; Kind et al., 2010; Prasad et al., 2013).

Here we report that ALADIN is required for timely chromosome alignment and spindle formation in human and Drosophila cells. We further show that this protein interacts with the inactive form of Aurora A and is required for the proper spatial regulation of this protein. Without ALADIN, we observe that a subset of Aurora A substrates within the spindle are mislocalized, producing spindles that are far less robust than those formed in control cells. We find similar defects in patient fibroblasts, which suggests that mitotic defects and/or misregulation of Aurora A may underlie some of the symptoms of triple A syndrome.

RESULTS

Previous studies showed that there is a strong link between the nuclear pore complex and mitotic spindle assembly. Our goal was to perform a comprehensive screen of all nucleoporins in Drosophila S2 cells to determine whether the known factors also play roles in mitosis in Drosophila and whether the roles of any novel factors have not yet been discovered. A previous whole-genome screen of all Drosophila proteins was carried out, but it failed to find any functions for Nups in mitosis (Goshima et al., 2007). Therefore we decided to take a more sensitive approach and looked at live cells, in which subtle defects in timing could be more easily detected, and we used a 5-d RNA interference (RNAi) treatment to more completely deplete the stable proteins of the nuclear pore complex (Boisvert et al., 2012). In our screen, we treated cells stably expressing green fluorescent protein (GFP)–histone H2B and mCherry–α-tubulin with double-stranded RNAs (dsRNAs) and then imaged the cells after 5 d. For every RNAi-treated sample, we imaged 12 individual fields of cells once per minute over the course of 2 h. In the resulting images, we could follow chromosome alignment and segregation, as well as mitotic spindle morphology, from prophase to telophase for several cells per dsRNA condition. Any depletion that appeared to perturb the formation of spindles or segregation of genomic material at anaphase was flagged for follow-up experiments. We additionally performed fixed-cell analyses of all depletions to visualize mitotic spindle morphology for a greater number of cells per treatment.

ALADIN depletion perturbs spindle formation

One of the strongest phenotypes we observed was produced by depleting the nucleoporin ALADIN (CG16892). In cells depleted of ALADIN, we noticed a striking delay in formation of the metaphase spindle (Figure 1, A and B). In ALADIN-depleted cells, the capture of kinetochores by microtubules was significantly delayed, but anaphase would still initiate after all chromosomes reached the metaphase plate (Figure 1A shows frames from these experiments). When we measured the length of metaphase spindles in our fixed samples, we noticed that they were significantly shorter than spindles in cells treated with control dsRNAs and were as short as spindles formed in the absence of the minus end–capping protein Patronin, which is known to influence spindle length (Goodwin and Vale, 2010). Codepleting Patronin and ALADIN did create somewhat shorter spindles, but this change was not significantly different from either single depletion (Figure 1C). Other than their shorter length, the morphology of the ALADIN-depleted spindles appeared to be largely normal (Figure 1D). A retrospective analysis of previous data from the whole-genome screen showed that ALADIN depletion produced a mild short-spindle phenotype, but the decrease in spindle length was not sufficiently great to be scored by the automated analysis program (Goshima et al., 2007). We confirmed that two separate nonoverlapping dsRNAs efficiently depleted ALADIN (as confirmed by quantitative reverse transcription [RT]-PCR) and produced short spindle phenotypes (Supplemental Figure S1).

ALADIN localizes around the mitotic spindle and at spindle poles in Drosophila and human cells

ALADIN has never been localized in Drosophila cells. To study its localization, we stably expressed GFP-ALADIN and mCherry–α-tubulin in S2 cells; as expected, the protein is clearly localized to the nuclear envelope in interphase (Figure 2A, top). ALADIN does not colocalize on kinetochores or discrete k-fiber bundles during mitosis (Figure 2A, bottom); instead, ALADIN localizes diffusely throughout the spindle, is excluded from chromatin, and is enriched on the remnants of the
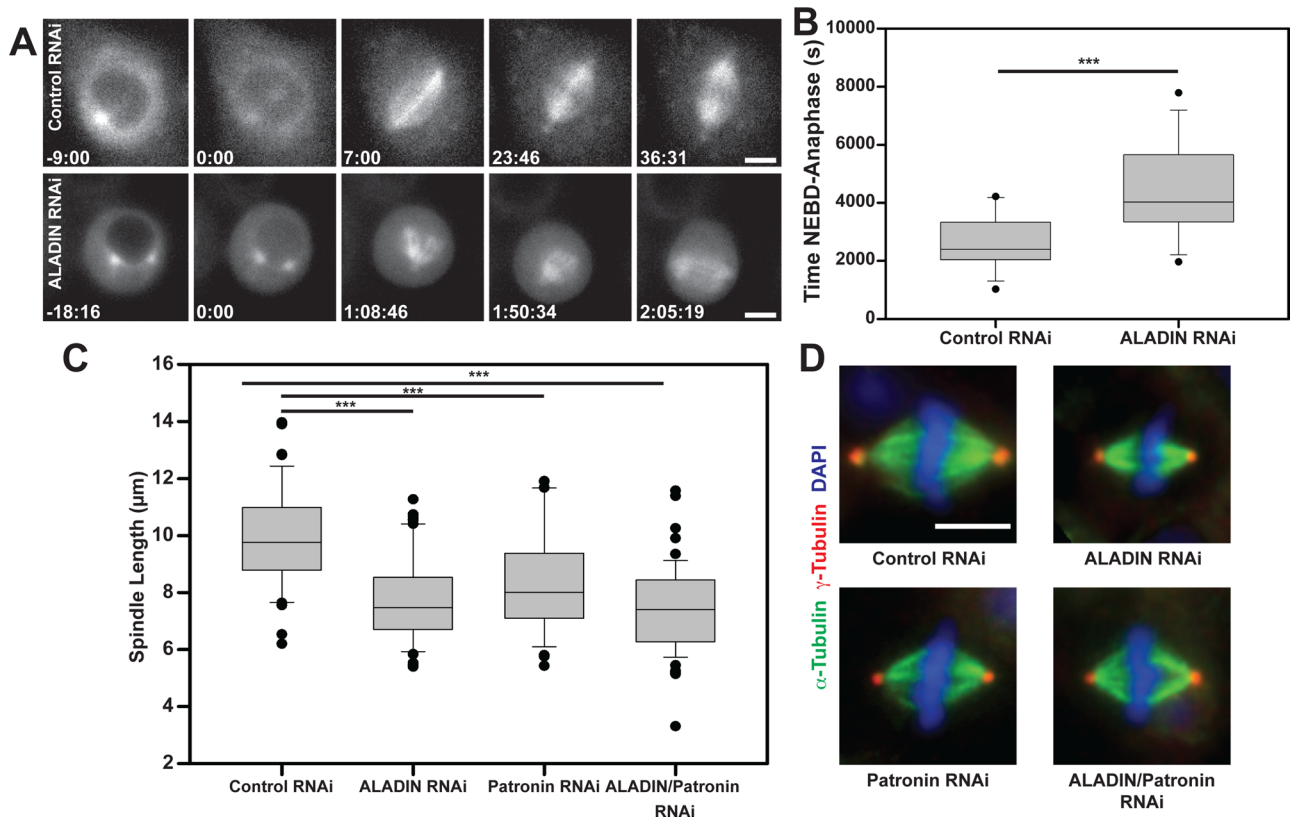
FIGURE 1: Depletion of ALADIN from *Drosophila* S2 cells impairs spindle assembly and produces shorter spindles. (A) Cells stably expressing mCherry–α-tubulin were treated with a dsRNA targeting GFP or ALADIN and then imaged with an automated microscope. Example images from time series of treated cells. (B) The time between nuclear envelope breakdown and anaphase onset was measured for multiple cells (*n* = 15 control and 12 ALADIN depleted). (C) Cells treated with the indicated dsRNAs were fixed and stained to visualize α-tubulin and γ-tubulin, and spindle length was measured for >35 spindles for each condition. (D) Example images for the four dsRNA treatments (red, γ-tubulin; green, α-tubulin; blue, DAPI). Box-and-whisker plots: box middle line shows the median; bottom and top lines show lower and upper quartiles (25 and 75%). Whiskers extend to the 10th and 90th percentiles, and all outliers (dots) are shown. Scale bars, 5 μm. ***p < 0.003.

nuclear envelope that surround the spindle. We also noticed that GFP-ALADIN is present in a ring that surrounds the centrosome in prometaphase and metaphase cells.

We wanted to know whether ALADIN had the same localizations in human cells. In interphase HeLa cells, GFP-ALADIN localizes to the nuclear envelope (Figure 2B, top; Cronshaw *et al.*, 2002), but its localization in mitosis has not been described. We therefore observed live HeLa cells stably expressing GFP-ALADIN that were transiently transfected with mCherry–α-tubulin. In metaphase cells, we observed a diffuse localization of GFP-ALADIN within the spindle with some accumulation around spindle poles, the highest concentration of which appeared to be between the centrosome and metaphase plate (Figure 2, B and C). Because ALADIN can interact with a transmembrane Nup that presumably remains with the mitotic endoplasmic reticulum (ER) remnant, we costained the GFP-ALADIN cells with an antibody that recognizes calnexin, an integral ER protein (Kind *et al.*, 2009; Figure 2C). We found that the high concentration of ALADIN that is proximal to the spindle pole colocalizes with calnexin and is therefore likely an ER membrane–associated pool of the protein. We wanted to know whether the localization of ALADIN around spindle poles was microtubule dependent, and so we treated cells with nocodazole to depolymerize microtubules. We found that in the absence of

microtubules, ALADIN did not appear to interact with centrosomes or chromatin.

ALADIN is required for proper spindle assembly in human cells

To determine whether ALADIN also has a role in spindle assembly in mammals, we treated HeLa cells with small interfering RNAs (siRNAs) that target human ALADIN (we used two nonoverlapping oligos that could deplete ~90% of the endogenous protein; Figure 3A). To synchronize cells in mitosis, we blocked RNAi-treated cells at the G2/M boundary with a CDK1 inhibitor (RO-3306) and released them into media containing MG132. After 2 h, cells were fixed and then stained to visualize microtubules, kinetochores, and DNA. Images from cells treated with control and ALADIN-specific siRNAs are shown in Figure 3B. We noticed that in the ALADIN-depleted cells, chromosomes on the metaphase plate appeared more disorganized. We measured the angle distribution of kinetochore pairs relative to the metaphase plate, as well as the interkinetochore distance, in control and ALADIN-depleted cells. To do this, we rotated the images of the spindles so that the metaphase plate was horizontal and perpendicular to the centrosomes, allowing us to measure the distance (*D*) between the outer edges of kinetochore pairs and the angle (θ) of the line connecting
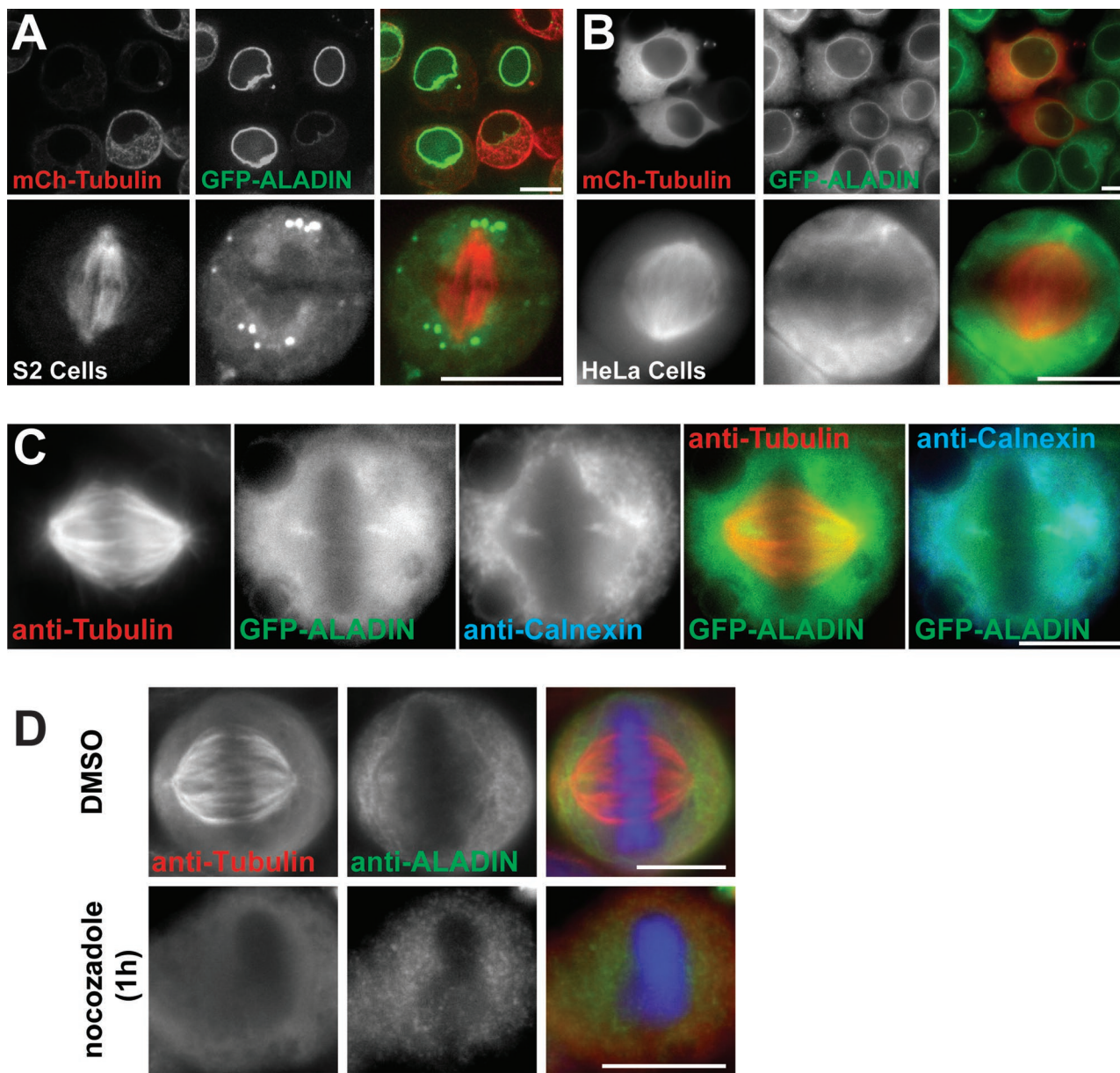
FIGURE 2: ALADIN localizes around the mitotic spindle and at the spindle poles in *Drosophila* and human cells. (A) *Drosophila* S2 cells expressing GFP-ALADIN and mCherry–α-tubulin in interphase (top) or metaphase (bottom). (B) Representative images of interphase (top) and metaphase (bottom) HeLa cells stably expressing GFP-ALADIN and transiently transfected with mCherry–α-tubulin. (C) GFP-ALADIN partially colocalizes with calnexin, an integral ER protein. (D) HeLa cells were fixed in the presence or absence of nocodazole and then stained to visualize tubulin and ALADIN. Scale bars, 10 μm.

the kinetochore pair with respect to the metaphase plate (Figure 3C). The ALADIN-depleted cells showed a significant 14% increase in interkinetochore stretch ($p < 0.001$) and a greater spread of kinetochore pair angles. In addition, depletion of ALADIN reduced spindle length by 5% (Figure 3D; $p < 0.05$). To quantify the disordered chromosome alignment, we measured the volume of the DAPI signal for each cell using a thresholding algorithm in Matlab that identified 4′,6-diamidino-2-phenylindole (DAPI)–positive pixels in each plane of a Z-stack of images (Otsu, 1979; Figure 3E) and observed a significant increase in chromatin area, confirming a disorganized metaphase plate. Consistent with the shorter spindle length, we also observed that the angle made by converging spindle microtubules (θ′ in the schema in Figure 3C) at

the pole was greater (10% increase, $p < 0.0001$) in the ALADIN-depleted cells (Figure 3F).

To determine whether human ALADIN is also required for proper timing of spindle assembly, we treated cells overnight with monastrol to generate monopolar spindles, washed out the inhibitor, fixed cells at 30, 45, and 60 min after washout, and then stained cells to visualize microtubules and DNA. Images of these samples were acquired, and individual cells were scored for their mitotic state (either prophase-prometaphase, metaphase, or anaphase-telophase). At 30 min after monastrol washout, both control and ALADIN-depleted cells were predominantly found to be in prophase-prometaphase (Figure 4A). After 45 min, the control sample showed a reduction in prophase-prometaphase cells and an
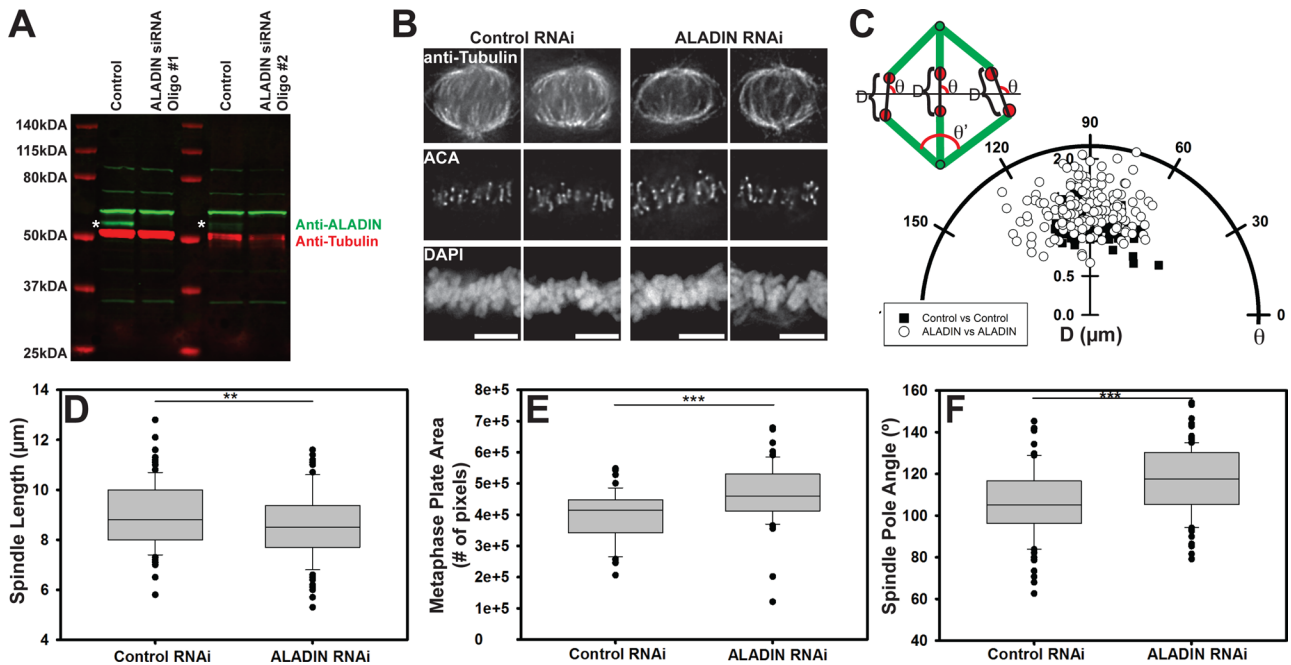
FIGURE 3: ALADIN is required for proper spindle morphology. (A) We observe efficient depletion of ALADIN with two different duplex oligonucleotides (see *Materials and Methods*). Tubulin levels were used as a loading control. Asterisks indicate ALADIN bands. (B) Representative control (left) and ALADIN-depleted (right) HeLa cell spindles. Cells were fixed and stained for microtubules (anti-tubulin), kinetochores (ACA), and chromosomes (DAPI). (C) Polar plot of the distance, *D*, and the angle, θ, between kinetochore pairs in control and ALADIN RNAi cells. Angles were calculated between the kinetochore pair and the metaphase plate after rotating the spindles in order to have the spindle poles perpendicular to the metaphase plate, as shown in the schematic representation. At least 200 measurements from several metaphase cells were made in each condition. (D) Cells treated with the indicated siRNAs were fixed and stained to visualize tubulin and chromosomes. ALADIN RNA-treated spindles are shorter than control spindles (8.983 vs. 8.560 μm). At least 100 spindles from four independent replicates were measured in each condition. (E) The area of DAPI signal across Z-stacks was measured at metaphase plates of fixed cells treated with control and ALADIN RNAi and incubated with MG132 for 4 h. Quantification was performed for at least 55 cells in each condition from three independent replicates. (F) Quantification of the angle (θ′; see schema in C) made by converging spindle microtubules at the poles in control and ALADIN-depleted cells (106.0 vs. 117.28°). At least 100 cells fixed and stained for microtubules were measured from three independent replicates. Scale bars, 5 μm. **$p < 0.05$ and ***$p < 0.0001$.

increase in anaphase-telophase cells; the ALADIN-depleted cells, however, did not show such a reduction in prophase-prometaphase cells until the 60-min time point, showing that ALADIN depletion also slows spindle assembly in human cells. We found that ALADIN-depleted cells arrested in mitosis with MG132 had more cells with Mad2-positive kinetochores (indicating unaligned kinetochores) and more Mad2-positive kinetochores per cell (Figure 4B), further confirming that chromosome alignment is delayed during mitosis.

We therefore examined the microtubules of the spindle to see whether they were affected by ALADIN depletion. Microtubules that attach to kinetochores become bundled into k-fibers, which are more stable than the populations of interpolar microtubules. To examine their stability in the absence of ALADIN, we placed control and ALADIN siRNA–treated cells on ice for 10 min before fixation. We then labeled these cells to visualize tubulin and chromosomes. ALADIN depletion led to a marked reduction of cold-stable k-fiber microtubules (Figure 4C). This reduction in k-fiber stability did not reflect an overall reduction in microtubule density; the average tubulin intensity in metaphase spindles was measured, but we found that in ALADIN-depleted cells, the tubulin intensity did not decrease (Figure 4D, 5% increase, $n = 3$ trials, >40 spindles per trial, $p < 0.10$).

To determine whether k-fibers are destabilized by an increase in the overall turnover (or flux) of microtubules within them, we depleted ALADIN from cells expressing photoactivatable GFP–α-tubulin (PA-GFP-tubulin) and then activated spots of PA-GFP-tubulin within the spindles of these cells. By measuring the decrease in fluorescence over time, we could determine how quickly microtubules are being polymerized and depolymerized. There are two populations of microtubules that can be visualized by this technique: a population that turns over rapidly (the interpolar microtubules) and a population that turns over with a longer half-life (k-fibers; Bakhoum *et al.*, 2009; Samora and McAinsh, 2011). Example plots are shown in Figure 4E for a control and an ALADIN-depleted cell. By fitting a double-exponential decay to the reduction in fluorescence after photoactivation for >24 cells/condition, we were able to extract the half-time of microtubule turnover for the fast (Figure 4F) and slow populations (Figure 4G). We did notice a trend of slightly slower flux for interpolar microtubules and faster flux for k-fiber microtubules after ALADIN depletion, but neither change was statistically significant. We therefore can exclude faster rates of microtubule depolymerization as being a major factor leading to the destabilization of k-fibers after ALADIN depletion.

Our observations that kinetochore stretch was increased after ALADIN depletion and that ALADIN never appears on kinetochores suggested that the connections between microtubules and kinetochores were unlikely to be perturbed in ALADIN-depleted cells.
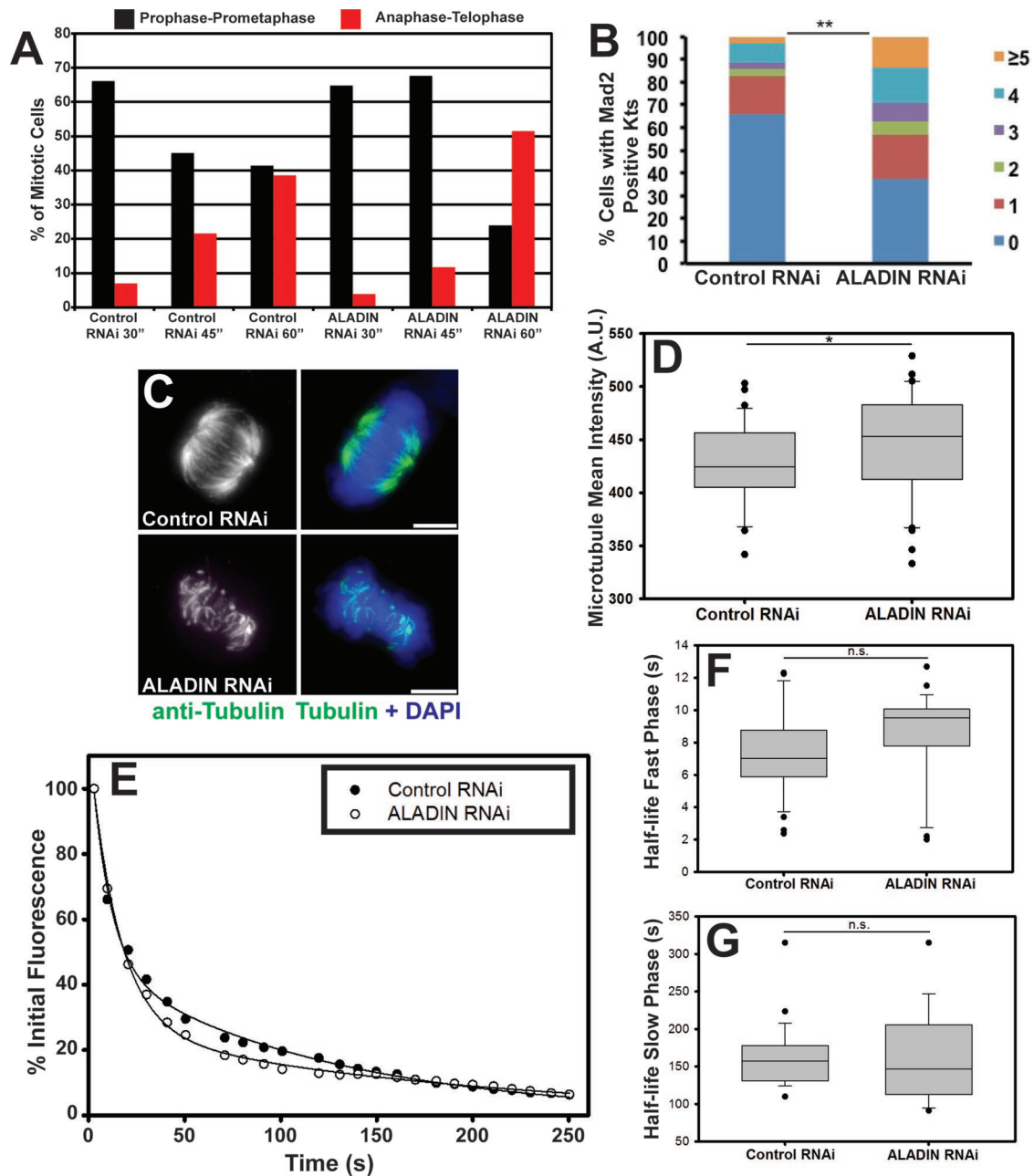
FIGURE 4: ALADIN is required for timely chromosome alignment and k-fiber stability. (A) Control and ALADIN-depleted cells were fixed and stained to visualize microtubules and DNA at the indicated times after monastrol washout. Mitotic cells were divided into three subclasses based on spindle and DNA morphology: prophase-prometaphase, metaphase, and anaphase-telophase; the percentages of cells within each subclass are plotted at the indicated time points. (B) Control and ALADIN-depleted cells incubated with MG132 were fixed and stained for Mad2 and ACA; the percentages of cells from two independent experiments with one, two, three, four, or five or more Mad2-positive kinetochore pairs are shown (**$p < 0.05$). (C) Representative maximum intensity projections of cold-treated control and ALADIN-depleted cells fixed and stained with anti–α-tubulin (green) and DAPI (blue). Scale bars, 5 μm. (D) Quantification of the microtubule density of fixed anti-tubulin–stained cells treated with control or ALADIN siRNAs. At least 40 microtubule spindle intensities were measured from three independent replicates (*$p < 0.1$). (E) Representative fluorescence intensity of PA-GFP-tubulin after photoactivation of spots within spindles of HeLa cells treated with the indicated siRNAs. Lines show fitting of a double-exponential curve to the decay of fluorescence. Box-plot of the half-time of microtubule turnover measured for the fast (F) and slow (G) phases from at least 24 cells in each condition from three separate biological replicates. ALADIN depletion does not induce a significant increase in the flux of interpolar microtubules (fast phase, 7.395 vs. 8.502 s, $p = 0.123$) or k-fibers (slow phase, 161.02 vs. 160.21 s, $p = 0.957$).
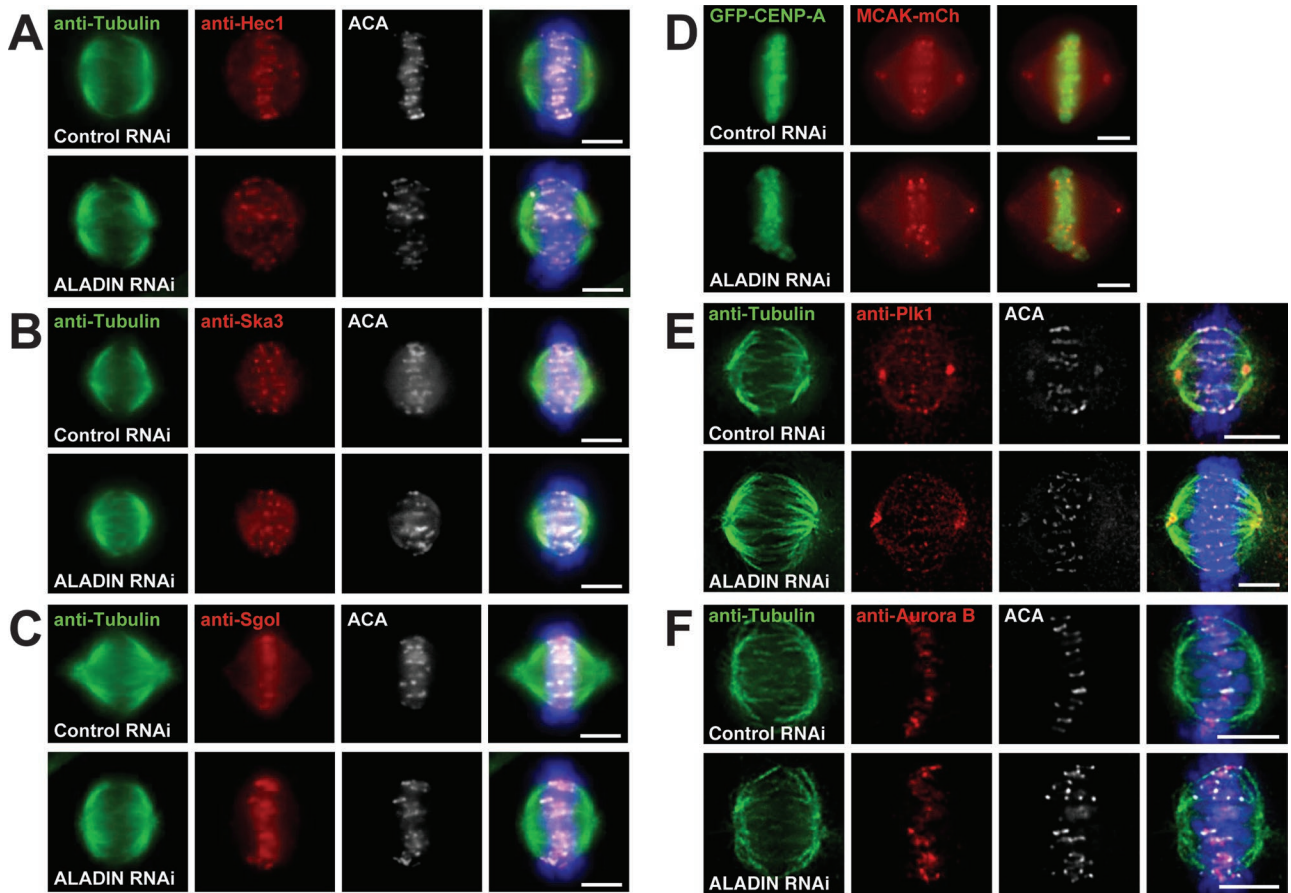
FIGURE 5: ALADIN depletion does not affect the targeting of multiple centromere and kinetochore proteins or the kinases Plk1 and Aurora B. (A–C) Representative Z-stack images of HeLa cells treated with control and ALADIN siRNAs that were fixed and labeled for microtubules (anti-tubulin, green), kinetochores (ACA, white) and the indicated proteins (red). (D) Representative live-cell images of control and ALADIN-depleted HeLa cells stably expressing MCAK-mCherry and GFP-CENP-A. (E, F) Representative Z-series images of cells treated with control or ALADIN-specific siRNAs and fixed and stained with antibodies that recognize tubulin, ACA, and Plk1 or Aurora B. Scale bars, 5 μm.

Staining of these cells with antibodies that recognize kinetochore and centromere proteins (Hec1, Ska3, and Sgo1) or visualizing a fluorescently tagged protein (MCAK) confirmed that the kinetochore structure did not appear to be grossly affected by ALADIN depletion (Figure 5, A–D).

ALADIN is essential for localizing AURORA A and NuMA to spindle poles

Mitotic kinases regulate multiple aspects of spindle function, and so we sought to determine whether any of the major mitotic kinases were mislocalized in ALADIN-depleted cells. We found that Aurora B and Plk1 were localized properly after ALADIN depletion (Figure 5, E and F). However, when we localized Aurora A in cells lacking ALADIN, we found that Aurora A spread outward from centrosomes and onto spindle pole microtubules, producing a 24% increase in the area of Aurora A–positive pixels (Figure 6, A and B).

Aurora A is activated by phosphorylation of threonine 288 (Littlepage *et al.*, 2002), and it is this form of the protein that regulates spindle assembly factors. When we examined the localization of the active form of Aurora A in control and ALADIN-depleted cells by quantitatively measuring the levels of phospho-T288 Aurora A, we found that ALADIN depletion reduces phospho-T288 Aurora A intensity at centrosomes by 38% (Figure 6C and Supplemental Figure S2A) while not reducing the overall levels of active Aurora A

(Figure 6D). Given that Aurora A is an important factor for centrosome function, we sought to ensure that the depletion of ALADIN was not affecting centrosome assembly. We therefore measured the intensity of pericentrin within mitotic centrosomes and found no difference between control and ALADIN-depleted cells (Figure 6E).

Because Aurora A regulates many spindle assembly factors and its full inhibition produces phenotypes that are much more extreme than what we observe after ALADIN depletion (Wang *et al.*, 2008; Asteriti *et al.*, 2011), we assumed that ALADIN has a partial role in regulating Aurora A function. To confirm this, we measured spindle length in control and ALADIN-depleted cells with and without treatment with the Aurora A–specific inhibitor MLN8237 (Figure 6F). We found that MLN8237 inhibition of Aurora A produces a more severe reduction in spindle length (35% reduction) than ALADIN depletion alone, confirming that removing ALADIN only partially inhibits Aurora A function; the reduction in spindle length we observed after MLN8237 treatment was not further augmented by ALADIN depletion. We also examined whether ALADIN overexpression could affect Aurora A activity and found that cells with high levels of ALADIN have less Aurora A on centrosomes and a higher level of the kinase on spindles (Supplemental Figure S2, C and D).

Aurora A has been shown to regulate many other spindle assembly factors (Tsai *et al.*, 2003, 2011; Bird and Hyman, 2008; Wong *et al.*, 2008; Zhang *et al.*, 2008; Jang *et al.*, 2009; Joukov *et al.*, 2010;
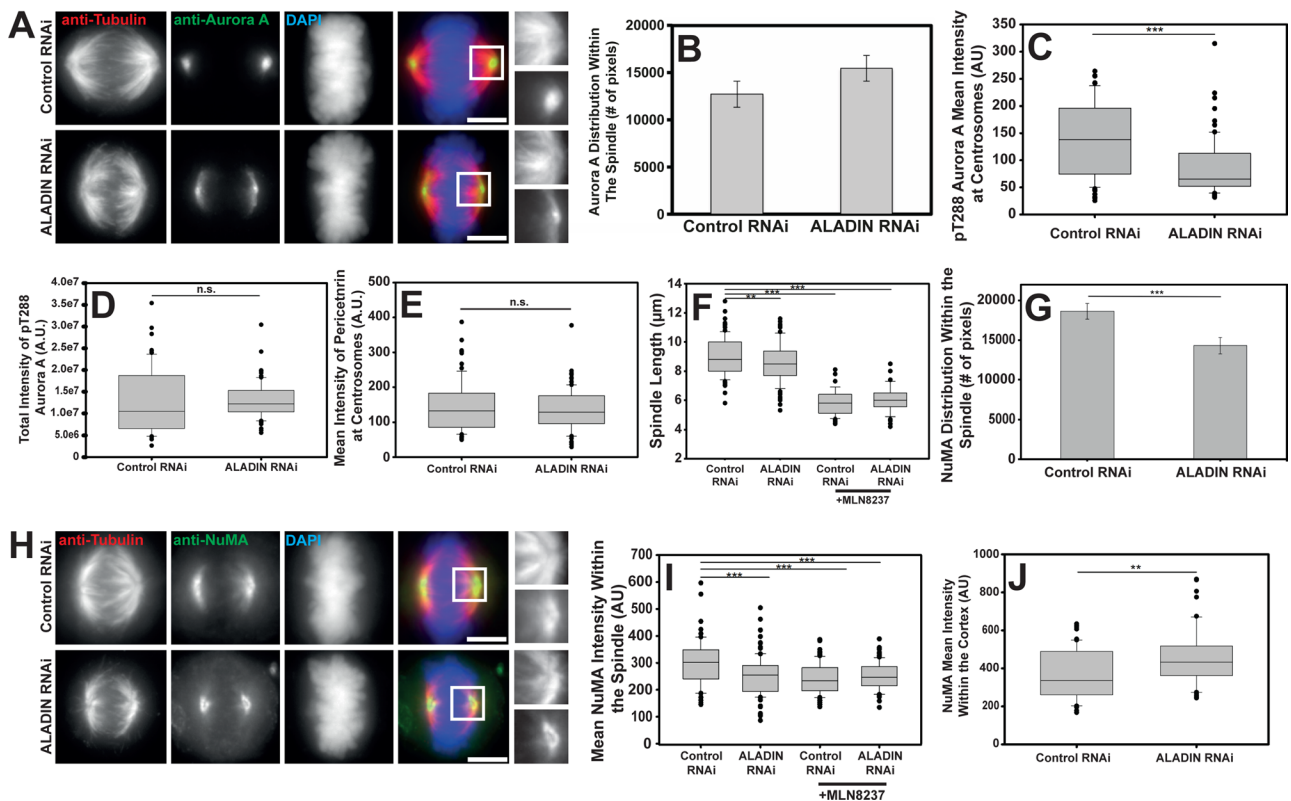
FIGURE 6: ALADIN is necessary for the proper localization and activity of Aurora A and NuMA. (A) Representative maximum intensity projections of Aurora A (green), tubulin (red), and DAPI (blue) in control and ALADIN-depleted cells. Shown for comparison are magnified views of microtubules (top) and Aurora A (bottom) from within the boxed regions in the merged images. (B) Quantification of the number of Aurora A–positive pixels within the spindle (12,714 vs. 15,478; mean ± SEM; at least 36 cells from four independent experiments). (C) Mean Aurora A activity at spindle poles in cells treated with the indicated siRNAs was quantitated using the phospho-T288 specific antibody. Pericentrin labeling was used to mark the centrosome, and phospho-T288 intensity was measured only under the pericentrin mask. At least 39 cells were measured in each condition from two independent replicates. (D) The total intensity of phospho-T288 Aurora A within cells treated with control or ALADIN-specific siRNAs as measured in Z-stacks. At least 79 cells were measured for each condition. (E) Mean intensity of pericentrin in cells treated with the indicated siRNAs (145.29 vs. 134.71) was measured; at least 39 cells from two replicates were measured for each condition. (F) Cells treated with the indicated siRNAs were incubated with or without MLN8237 and then fixed and stained to visualize α-tubulin and chromosomes. Spindle length was measured for >46 spindles for each condition across three replicates. (G) Quantification of the number of NuMA-positive pixels within spindles of cells treated with the indicated siRNAs (mean ± SEM; at least 35 cells measured from four independent replicates). (H) Representative maximum intensity projection of control and ALADIN-depleted HeLa cells fixed and stained to visualize tubulin (red), NuMA (green), and DAPI (blue). Also shown are magnified views of microtubules (top) and NuMa (bottom) from within the boxed regions in the merged images. (I) ALADIN depletion reduces the average NuMA intensity within the spindle in a manner similar to Aurora A inhibition. Control or ALADIN-specific siRNA–treated cells were incubated or not for 40 min in MLN8237 and then fixed and stained to visualize NuMA and microtubules. Average NuMA intensity was measured within the spindle of at least 33 cells from four biological replicates (mean intensities 297.9, 253.2, 240.1, and 251.8). (J) Mean intensity of NuMA on the polar cortex was measured in control and ALADIN-depleted metaphase cells. At least 50 cells were measured for each condition. Box-and-whisker plots: box middle line shows the median and the bottom and top lines show the lower and upper quartiles (25 and 75%). Whiskers extend between the 10th and the 90th percentiles, and all outliers (dots) are shown. **$p < 0.003$, ***$p < 0.0001$, n.s. nonsignificant.

Rome *et al.*, 2010; Asteriti *et al.*, 2011; Cheeseman *et al.*, 2011; Lioutas and Vernos, 2014), and we sought to determine which of these may be affected by the change in Aurora A localization produced by depleting ALADIN. We found that the localization of the microtubule minus end–binding protein NuMA changed noticeably after ALADIN was depleted (Figure 6H). The protein appeared to be less spread around the spindle pole and was more constricted to an area just around the centrosome. When we quantified the area of the spindle covered by NuMA, we found that the area decreased by 23% (Figure 6G) and the average fluorescence intensity within the spindle

also decreased by 15% (Figure 6I). We wanted to know whether ALADIN depletion was affecting the levels of Aurora A and NuMA protein, and so we made lysates from control and ALADIN-depleted cells and probed these lysates to detect the total levels of ALADIN (to confirm depletion), NuMA, and Aurora A. There was no reduction of Aurora A or NuMA when ALADIN protein levels were substantially reduced (Supplemental Figure S2B). We sought to determine whether the relocalization of NuMA seen in ALADIN-depleted cells was caused by reductions in Aurora A activity, and so we examined the localization of NuMA in control and ALADIN-depleted cells with
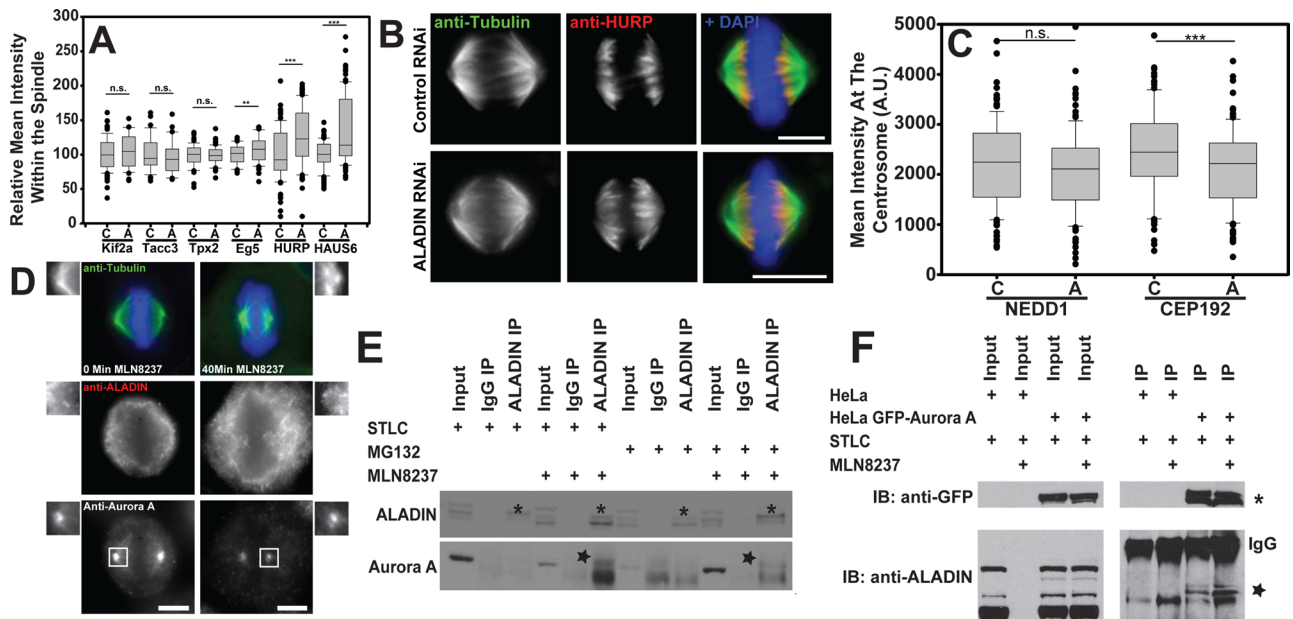
FIGURE 7: Aurora A binds to ALADIN, and its substrates show different sensitivity to ALADIN depletion. (A) The fluorescence intensities of the indicated spindle assembly factors in control, C, and ALADIN-depleted, A, cells were measured and normalized, and only the localizations of Eg5 (0.802 vs. 0.859), HURP (0.485 vs. 0.607), and HAUS6 (0.680 vs. 0.925) were affected by ALADIN depletion. All experiments were done three times, with the exception of Kif2a and HAUS6 ($n = 2$) and HURP ($n = 4$); at least 36 cells were measured in each condition. (B) HeLa cells were treated with control and ALADIN-specific siRNAs and then fixed and labeled for microtubules (green), HURP (red), and chromosomes (blue). (C) The levels of centrosomal NEDD1 and CEP192 were quantitated on centrosomes in cells treated with control, C, and ALADIN-specific, A, siRNAs ($n > 135$ spindles per condition). (D) HeLa cells were treated with MLN8237 to inhibit Aurora A activity. Cells were then fixed and stained to visualize ALADIN, Aurora A, microtubules (green), and DNA (blue). (E) Cells were arrested at either prophase/prometaphase (+STLC = overnight treatment with STLC) or metaphase (+MG132 = overnight treatment with RO-3306 and release into MG132 for 4 h) and treated or not with MLN8237 before making lysates that were incubated with either a species-specific IgG or anti-ALADIN antibodies coupled to protein A–agarose beads. The blot shows that we could precipitate ALADIN in all conditions, but Aurora A was only coprecipitated when it was inhibited. Asterisks show the ALADIN-specific band, and the star shows the Aurora A–specific band. (F) Cells transiently transfected with GFP or stably expressing Aurora A-LAP were treated with STLC overnight, and half were also treated with MLN8237 to inhibit ALADIN. We observe greater ALADIN coimmunoprecipitation when Aurora A is inhibited. Scale bars, 10 μm. **$p < 0.05$; ***$p < 0.001$.

or without treatment with MLN8237. The intensity of NuMA staining within the spindle was decreased similarly by ALADIN depletion, Aurora A inhibition, and a combination of both treatments (Figure 6I), suggesting that NuMA's redistribution within the spindle may be due to the observed change in Aurora A activity after ALADIN depletion.

In addition to its localization on spindle poles, NuMA also interacts with the cell cortex, where it helps to position the mitotic spindle. We found that there was a 22% increase in the cortical localization of NuMA when ALADIN is depleted (Figure 6J). NuMA interacts with the minus end–directed motor protein dynein (Merdes *et al.*, 1996), and we found that the depletion of ALADIN also reduced the concentration of the dynein cofactor dynactin within the spindle by 12.7%, as judged by the localization of GFP-p150 stably expressed from a BAC clone using the endogenous promoter (Poser *et al.*, 2008; unpublished data).

ALADIN is an Aurora A–binding protein that regulates the localization of a specific subset of Aurora A targets

We examined the localization of several other Aurora A substrates and found that the depletion of ALADIN produced striking increases in the amount of HURP and the Augmin subunit HAUS6 within the spindle while producing a modest effect on Eg5/Kif11 localization. Kif2a, TACC3, and Tpx2 were unaffected by ALADIN depletion

(Figure 7A and Supplemental Figure S3). The relocalization of HURP was particularly interesting. Unlike NuMA, which is reduced on the spindle, HURP spreads along the spindle after ALADIN depletion; this relocalization may be influenced by active Aurora A spreading from spindle poles onto the spindle (Figure 7B).

Aurora A is activated on spindle microtubules by Tpx2 and on centrosomes by CEP192 (Joukov, 2011; Hochegger *et al.*, 2013; Chen *et al.*, 2014). To determine whether defects in the centrosome assembly could account for the reduction of active Aurora A at the centrosome, we evaluated the localization of CEP192 and NEDD1 on centrosomes. We found that CEP192 levels were reduced by 12%, whereas NEDD1 levels did not change at all (Figure 7C). NEDD1 localization depends on Plk1 phosphorylation of Nek9, and Plk1 activation requires Aurora A (Sdelci *et al.*, 2012; Joukov *et al.*, 2014). This suggests that the original centrosomal activation of Plk1 is not perturbed in ALADIN-depleted cells and that the decrease of active Aurora A at the centrosome does not reflect an overall defect in centrosome assembly.

Observing that the reduction of ALADIN levels can influence the localization of active Aurora A and some of its substrates, we sought to determine whether this Nup is influenced by the kinase. ALADIN shows a mild enrichment around spindle poles in metaphase cells, but we found that treatment with MLN8237 increased the polar
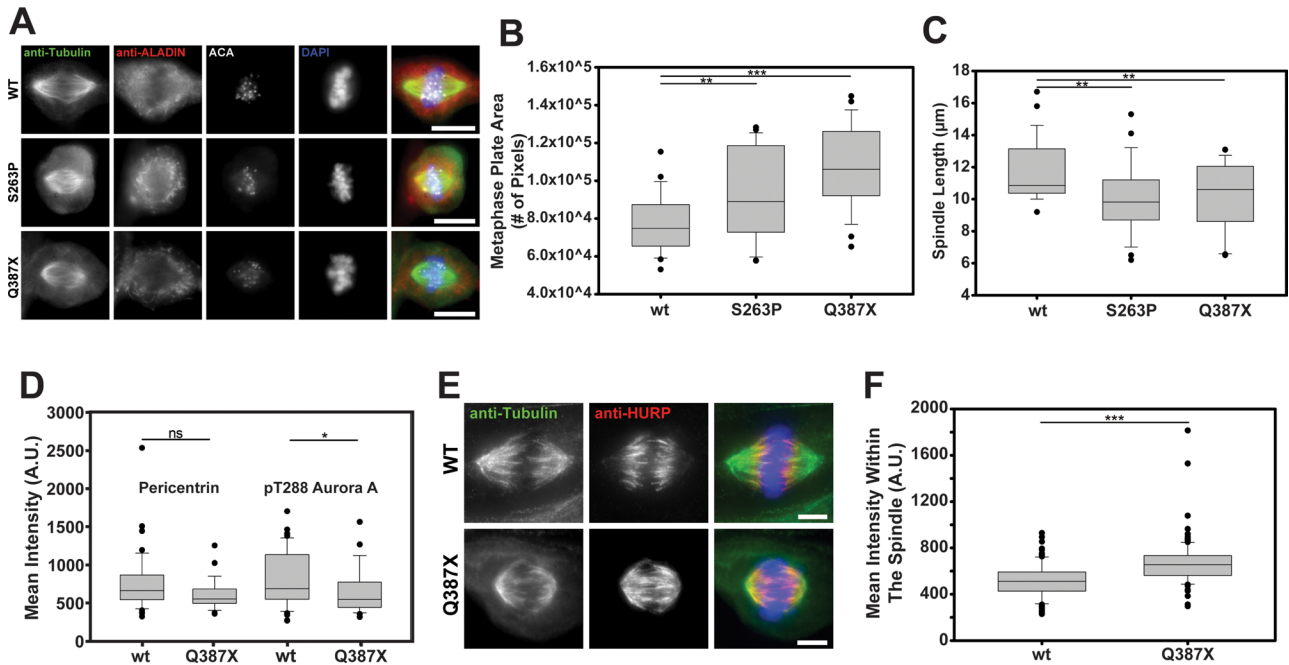
FIGURE 8: Triple A patient fibroblasts show errors in spindle assembly, and the ALADIN disease mutants localize differently than the wild-type protein. (A) Control fibroblasts and fibroblasts from patients expressing two different disease mutant forms of ALADIN, p.S263P and p.Q387X, were fixed and stained to visualize the spindles. The metaphase plate area (B) ($n = 24$ for wild type, 26 for S263P, and 27 for Q387X) and spindle length (C) ($n = 26$ for wild type, 27 for S263P, and 25 for Q387X) were measured for the three fibroblast populations. (D) Wild-type and Q387X patient fibroblasts were fixed and stained to visualize pericentrin and active Aurora A. The mean amount of pericentrin was measured at centrosomes for both cell types, and then the amount of active Aurora A was measured under a mask generated by pericentrin ($n = 42$ for wild type and 29 for Q387X). (E) HURP was visualized in mitosis in control and patient fibroblasts. (F) The mean intensity of HURP was measured within spindles formed in control and patient fibroblasts ($n > 100$ spindles from three independent replicates). *$p < 0.04$, ** $p < 0.006$, and ***$p < 0.0000006$. n.s., not significant. Scale bar, 5 μm.

accumulation of ALADIN (Figure 7D) while also reducing the amount of Aurora A on spindle microtubules. Therefore Aurora A activity appears to regulate ALADIN's localization. To determine whether ALADIN could interact with Aurora A, we immunoprecipitated ALADIN from cells arrested in either prophase/prometaphase (overnight treatment with STLC) or metaphase (overnight treatment with RO-3306 and then release into media with MG132 for 4 h) in the presence or absence of MLN8237. We could detect the coprecipitation of Aurora A in both mitotic states, but only when Aurora A was inhibited, suggesting that ALADIN preferentially interacts with the inactive form of this kinase (Figure 7E). In addition, we could coprecipitate ALADIN when we immunoprecipitated Aurora A–GFP that was stably expressed from a BAC clone using the endogenous promoter, which was enhanced when cells were treated with MLN8237 (Figure 7F).

Mitotic errors are common in triple A patient fibroblasts
Problems with cell cycle timing have been reported in fibroblasts from triple A patients. However, the mitotic spindle has never been examined in these cells. We therefore cultured fibroblasts from patients homozygously expressing the p.S263P and p.Q387X mutant forms of ALADIN. We observed that the mutant fibroblasts both showed disorganized metaphase plates and shorter metaphase spindles compared with control fibroblasts (Figure 8, A–C). The localization of active Aurora A on centrosomes was also measured in these cells. Because these cells are very slowly dividing, we had difficulty in getting many mitotic cells to analyze. The Q387X mutant cells showed

a reduction in phospho-T288 Aurora on centrosomes (without any change in pericentrin localization; Figure 8). We also observed that the distribution and amount of HURP within the spindle was significantly altered in the Q387X mutant cells. HURP spread poleward and was more concentrated on spindle microtubules (Figure 8).

The localization of the mutant proteins did not seem so different from that of the wild type (Figure 8A). However, to determine whether these proteins behave similarly to the wild type, we treated cells with MLN8237. We found that the ALADIN S263P mutant protein concentrated around spindle poles when Aurora A was inhibited, similar to the wild-type protein, but the Q387X mutant did not (Supplemental Figure S4).

DISCUSSION
ALADIN has been studied in the context of the functioning of adrenal and neuronal cells in triple A syndrome, and many of the phenotypic features seen in triple A patients have been ascribed to this protein's role in nucleocytoplasmic transport. We show for the first time that this protein also has functions in cell division, during which it is required to build spindles that assemble with wild-type timing, are of the proper length, and have stable k-fiber microtubule bundles.

The activation and localization of Aurora A have previously been shown to be controlled by many other accessory proteins (Bayliss et al., 2003; Eyers and Maller, 2003; Hirota et al., 2003; Zhao et al., 2005; Hutterer et al., 2006; Dodson and Bayliss, 2012; Reboutier et al., 2012; Silva and Cassimeris, 2013; Lioutas and Vernos, 2014). We demonstrated that ALADIN is a novel Aurora A cofactor that

promotes the localization of the active form of this kinase at centrosomes. Aurora A dynamically associates with the centrosome, and we found that both reducing and increasing ALADIN protein levels led to a diminished amount of active centrosomal Aurora A (Conduit et al., 2014). Given these data and the fact that ALADIN preferentially interacts with inactive Aurora A, we hypothesize that ALADIN could act to locally anchor inactive Aurora A that is released from spindle poles and promote its reactivation by other cofactors. However, an overabundance of ALADIN could outcompete these factors and prevent the subsequent reactivation and recruitment of the active kinase to the centrosome. Our finding that a specific subset of Aurora A substrates (NuMA, HURP, and Augmin) is affected by the redistribution of active Aurora A from centrosomes onto spindles, whereas many others (Plk1, Kif2a, TACC3, and Tpx2) are not, demonstrates that there are multiple, separable pathways by which Aurora A can regulate its substrates and reinforces the idea that the spatial regulation of this kinase is essential for its proper function. A spindle matrix built of components including vesicles, lamins, and nucleoporins has been proposed to function as a nonmicrotubule scaffold that can concentrate and/or activate spindle assembly regulators (Zheng, 2010; Schweizer et al., 2014). Although we cannot say anything definitive about the existence or function of the spindle matrix, ALADIN's localization and role in regulating Aurora A function are both consistent with the proposed nature of a matrix component.

Although the depletion of ALADIN perturbs the localization of NuMA, the phenotype we observed is quite different from a total loss of NuMA (Silk et al., 2009), suggesting that there is still NuMA function in the absence of ALADIN. Because the NuMA localization phenotype is similar in cells lacking ALADIN, when Aurora A activity is inhibited, or where the Aurora A phosphosite is mutated to alanine (Kettenbach et al., 2011), we hypothesize that ALADIN depletion leads to the hypophosphorylation of NuMA and reduces but does not eliminate its function in spindle focusing.

There is an intriguing interaction between NuMA and the nucleoporin Nup188 that is required for the proper localization of NuMA at the spindle poles (Itoh et al., 2013). We cannot rule out that Aurora A also regulates Nup188 and that the NuMA phenotype we observe is downstream of a misregulation of Nup188, but given our observations that Aurora A can interact with ALADIN and that overexpression and depletion of ALADIN both perturb the distribution of active Aurora A, we favor a model in which ALADIN regulates NuMA through its effects on Aurora A.

In addition to affecting NuMA localization, ALADIN, through its regulation of Aurora A's distribution, also appears to regulate the localization of HURP and the Augmin complex. HURP localization is controlled by both a Ran-GTP–dependent release from importin β and Aurora A phosphorylation (Sillje et al., 2006; Wong et al., 2008). We did not see any defects in Tpx2 localization in ALADIN-depleted cells, which indicates that the Ran gradient was not severely perturbed in cells lacking ALADIN. Thus we believe that the poleward spread of HURP is due to the spread of Aurora A activity onto spindle microtubules.

The regulation of Augmin by Aurora A is not as clearly defined, since this kinase promotes the localization of NEDD1 within the spindle but inhibits Hice1 microtubule binding (Tsai et al., 2011; Pinyol et al., 2013). However, given that we see a marked increase in HAUS6 but no real change in microtubule density within ALADIN-depleted spindles, we believe that the perturbation of Aurora A activity caused by ALADIN depletion induces Augmin recruitment but does not necessarily increase its activity. Taken together, our data suggest that ALADIN depletion spatially alters Aurora A activity to selectively change the distribution of a specific suite of spindle assembly and stabilizing factors within the spindle. We hypothesize that when ALADIN is removed, the resulting change in the stoichiometry of microtubule-binding factors produces the increased kinetochore stretch, destabilized k-fibers, and delayed chromosome alignment that we observed.

It is not immediately obvious how both the overrecruitment of HURP to the spindle and increased kinetochore stretch are seen in spindles that are less stable. HURP association with the spindle normally stabilizes the k-fiber microtubules (Sillje et al., 2006). In addition, increased kinetochore tension usually boosts microtubule binding (King and Nicklas, 2000). Meunier and Vernos (2011) did report that depletion of MCRS1, which caps microtubule minus ends, produced a very similar phenotype of shorter, destabilized spindles with hyperstretched kinetochores. However, they did not report on HURP localization in MCRS1-depleted cells, and they showed that, unlike what we observe for ALADIN, MCRS1 regulates microtubule flux during metaphase (Meunier and Vernos, 2011). Considering these results with our own, we hypothesize that there are multiple ways in which tension within the spindle may be dysregulated and that when the normal distribution of assembly factors is disturbed, proteins that promote spindle stability can have the opposite effect.

During normal cell cycles, none of the defects we see after ALADIN depletion are enough to block cell divisions. In addition, because the ALADIN-knockout mouse and patients expressing mutant forms of the protein, including p.G14fs and p.W84X, which may both be functionally null, are viable, we can assume that most cell types can divide without ALADIN (Huebner et al., 2006; Krumbholz et al., 2006). We observed that once ALADIN-depleted cells complete chromosome alignment, they progress to anaphase without lagging chromosomes or other hallmarks of mitotic errors. In most cells, ALADIN's role in regulating Aurora A function makes spindle assembly more robust. However, it is possible that this role becomes more critical in different tissue types.

It has been proposed that alterations in reactive oxygen levels or defects in nucleotide excision repair produce the symptoms seen in patients who suffer from triple A syndrome (Kiriyama et al., 2008; Storr et al., 2009; Kind et al., 2010; Prasad et al., 2013). We show for the first time that the expression of two mutant forms of ALADIN in patient cell lines produces specific defects in mitotic spindle formation. It was of interest to observe that although the expression of both mutant ALADIN isoforms perturbs spindle formation, only one of the isoforms is defective in its localization after Aurora A inhibition. This suggests that the S263P mutant protein retains some mitotic functions and may explain why the expression of this mutant form of ALADIN rescues female sterility and spindle assembly defects seen in oocytes from the ALADIN-knockout mouse (Huebner et al., 2006; Carvalhal, unpublished data). Further work is needed to determine to what extent mitotic spindle assembly errors contribute to the etiology of triple A syndrome either alone or in combination with deficits in DNA repair or reactive oxygen/superoxide homeostasis that have already been documented in patient cells.

MATERIALS AND METHODS
Cell culture, siRNA, plasmid transfections, and drug treatments
Drosophila cells stably expressing mCherry–α-tubulin and GFP-H2B were grown in Express Five medium supplemented with 1× antibiotic-antimycotic and glutamine (Life Technologies). ALADIN was depleted by the method of Rogers and Rogers (2008) using two nonoverlapping dsRNAs generated from PCR templates created with the primer sets TGAATAGTCTGCAATTATGGCG and GAACTGAGCAATACGCTCTGC or GAAGTGGTCGCCGGATAAT and

AGCAGACTCTGTTGCACGAA (all primers also contained 5′ T7 binding sites) and transcribed using a Megascript T7 transcription kit (Life Technologies). To quantify the mRNA depletion, total RNA was isolated with the RNeasy kit (Qiagen), and cDNAs were created with the Superscript III First-Strand Synthesis System for RT-PCR (Life Technologies) using the Oligo(dT)20 primer. Two-step quantitative PCRs of diluted cDNA samples were performed using 2× Brilliant SYBR LowRox Master Mix (Agilent) on a RotorGene6000 instrument. ALADIN mRNA depletion was confirmed using Rpl32 as a control template, which did not change after ALADIN dsRNA treatment (primers CGAGATCGTGATAGGTTGTCGG and GAGGTTATTG-GCAGATTGTTTGG were used to amplify the ALADIN message, and ATGCTAAGCTGTCGCACAAATGGC and GTGCGCTTGTTC-GATCCGTAACC were used for Rpl32). The sequence of primers used to deplete Patronin was previously published (Goodwin and Vale, 2010).

The fibroblast cell lines (p.S263P, p.Q387X, and wild-type ALADIN) were previously described (Kind et al., 2010). The HeLa cell line stably expressing GFP-ALADIN was previously described (Kind et al., 2009), and the HeLa cell line stably expressing cell PA-GFP–α-tubulin and RFP-H2B was a gift from A. McAinsh (University of Warwick, Coventry, United Kingdom; Samora and McAinsh, 2011). GFP-p150 and Aurora A-LAP were expressed from a BAC clone using the endogenous promoter, a gift from A. Hyman (Max Planck Institute for Molecular Cell Biology and Genetics, Dresden, Germany; Poser et al., 2008). All cell lines were grown in Opti-MEM plus GlutaMAX supplemented with 10% fetal bovine serum, 100 U/ml penicillin, and 100 μg/ml streptomycin at 37°C with 5% CO_2 in a humidified incubator, with the exception of fibroblasts, for which DMEM plus GlutaMAX was supplemented with 0.25 μg/ml amphotericin B (all media and supplements were from Life Technologies).

To deplete ALADIN, 2.5×10^5 cells were reverse transfected with 70 nM duplex oligonucleotides 5′-UGAGUUUGCAAUUUCAU-UUAGCACC-3′ and 5′-AUCUCUUCCACACUUGCUCCCGGUG-3′ (stealth RNAi; Life Technologies and Sigma-Aldrich) using Lipofectamine RNAiMAX (Life Technologies) for 48 h, with a second RNAi forward transfection after 24 h. A low-GC duplex siRNA (Life Technologies) was used as negative control. During transfection, cells were maintained in antibiotic-free complete culture medium.

FuGENE HD transfection reagent (Promega) was used for transfections of GFP-ALADIN (Krumbholz et al., 2006) or an empty GFP vector (pEGFP-C1; Clontech) according to the manufacturer's instructions. Typically, cells were transfected with a ratio of 3:1 transfection reagent:DNA for 48–72 h before assaying.

To increase the number of mitotic cells for immunostaining, cells were incubated with either 10 μM MG132 (Calbiochem) for 4 h or 2.5 ng/ml RO-3306 overnight to arrest them at the G2/M border before releasing them into MG132 for 2 h before fixation. For live-imaging experiments or Western blot analysis, cells were treated with 2.5 ng/ml RO-3306 (Calbiochem), 5 μM S-trityl-L-cysteine (STLC; Enzo Life Sciences), or monastrol for 16–20 h. If metaphase arrest was required, cells were treated with MG132 for 2 h after the removal of RO-3306. For Aurora A inhibition, cells were treated with 1.5 ng/ml MLN8237 for 40 min (Selleckchem).

Live-cell imaging
S2 cells were imaged on an ASI MIM-RAMM microscope (Applied Scientific Instrumentation) outfitted with a Lumencor Sola LED light engine (Lumencor), ASI FW-1000 excitation and emission filter wheels with appropriate 25-mm–band-pass filters (Chroma Technology), a 40×/0.95 numerical aperture (NA) objective (Olympus), and

a Photometrics HQ2 camera (Photometrics). Images were acquired with μManager software (www.micromanager.org).

All live-cell imaging of HeLa cells was performed on a DeltaVision microscope (Applied Precision) outfitted with an environmental chamber to maintain 37°C, and cells were imaged in Leibovitz's L-15 medium supplemented with 10% fetal bovine serum, 100 U/ml penicillin, and 100 μg/ml streptomycin.

For analysis of tubulin poleward flux, metaphase HeLa cells stably expressing PA-GFP–α-tubulin and RFP-H2B and arrested at metaphase with MG132 were identified by the RFP-H2B fluorescence. Microtubules adjacent to the metaphase plate on one side of the spindle structure were photoactivated with a 50-ms pulse from a 406-nm laser (60% power). Images were acquired using an Olympus 100×/1.35 NA lens with 200-ms exposures using the adaptive intervals program in SoftWoRx (Applied Precision). Fluorescence intensities were measured with Fiji and normalized to the background. Microtubule turnover half-lives for each cell were calculated by fitting a double-exponential curve as described in Samora and McAinsh (2011).

Immunofluorescence microscopy and antibodies used
Cells grown on 22 × 22 mm #1.5 coverslips were fixed with warm 4% formaldehyde (Electron Microscopy Sciences) in 1× PHEM for 5 min, followed by 5-min permeabilization with PHEM plus 0.5% Triton X-100 (Roche) and then fixed again. For cold assay analysis, cells were fixed in prechilled 90% methanol, 1.6% formaldehyde, and 5 mM sodium bicarbonate, pH 9, for 10 min at –20°C. After fixation and permeabilization, coverslips were incubated for 5 min in PHEM plus 0.1% Triton X-100 (PHEM-Wash), Tris-buffered saline (TBS) plus 0.1% Triton X-100, and again in PHEM-Wash. Blocking and antibody dilution buffer was TBS, 0.1% Triton X-100, 2% bovine serum albumin, and 0.1% sodium azide. Coverslips were blocked for 30 min at room temperature (25°C), primary antibody incubations were done overnight at 4°C, and secondary antibody incubations were done at room temperature for 2 h. Excess antibodies were removed after primary and secondary antibody incubations by three washes with PHEM-Wash for 5 min. Coverslips were mounted in Dako Fluorescence Mounting Medium (Dako) and sealed using CoverGrip Coverslip Sealant (Biotium). To assay for k-fiber microtubule stability, cells were placed for 10 min on a solid aluminum block resting on ice.

Fixed cells were imaged on a Delta-Vision Core microscope (Applied Precision) with a 100× oil-immersion 1.35 NA objective lens (Olympus), a CoolSNAP HQ camera (Photometrics), and standard filter sets. Three-dimensional images were acquired with SoftWoRx software (version 5.5.0; Applied Precision), and Z-series optical sections were recorded with slices taken every 0.2 μm.

Quantitative analysis of fluorescence microscopy data was performed using OMERO software (Open Microscopy Environment; Allan et al., 2012) and OMERO.mtools, a MATLAB (MathWorks) plug-in (www.openmicroscopy.org/site/products/partner/omero.mtools). For the analysis, DeltaVision files were imported into OMERO, and masks of regions of interest were created by defining the Otsu threshold of the α-tubulin signal (spindle mask) or the pericentrin signal (centrosome mask). Measurements of average intensity/pixel across Z-series for each experiment were calculated in each channel within the mask regions defined. Relative mean intensity values or pixel numbers were obtained after correcting for the background fluorescence. For spindle-length measurements, pole–pole distance was measured using OMERO. To measure pole focusing, angles were measured manually for each pole stained for tubulin using Fiji. To measure kinetochore–kinetochore distances, single image planes

were selected for which kinetochore pairs were clearly resolved, and the distance between pairs was measured with OMERO. To quantify chromosome alignment, the volume of the metaphase plate of each cell, the pixel area across Z-series, was calculated using the Otsu threshold of the 4′,6-diamidino-2-phenylindole (DAPI) signal using OMERO.mtools.

The following antibodies were used for immunofluorescence (IF) and Western blot studies: rat anti–α-tubulin at 1:200 for IF (Pierce), mouse anti–α-tubulin at 1:1000 for IF (Sigma-Aldrich), human anti–ANA centromere CREST at 1:1000 for IF (Fitzgerald), rabbit anti-calnexin 1:75 for IF (Cell Signaling), rabbit anti-Kif2a at 1:1000 for IF (a gift from D. A. Compton, School of Medicine at Dartmouth, Hanover, NH), rabbit anti–Ska-3 at 1:500 for IF (a gift from A. SantaMaria, University of Basel, Basel, Switzerland), rabbit anti-HAUS6 at 1:200 for IF (a gift from L. Pelletier, Lunenfeld Research Institute, Toronto, Canada), rabbit anti–phospho-Hec-1 at 1:500, mouse and rabbit anti-pericentrin at 1:500 and 1:1000 for IF and mouse anti-plk1 at 1:1000 for IF (all gifts from J. Swedlow, University of Dundee, Dundee, United Kingdom), rabbit anti–Cep192 at 1:200 and mouse anti-NEDD1 1:1000 for IF (both gifts from S. Rocha, University of Dundee), rabbit anti-ALADIN 1:1000 for blotting and 1:200 for IF (Proteintech Europe), mouse anti-ALADIN at 1:100 for IF (monoclonal B-11; Santa Cruz Biotechnology), rabbit anti-NuMA at 1:1000 for IF and 1:2000 for blotting, rabbit anti-TPX2 at 1:1000 for IF, rabbit anti-Eg5 at 1:1000 for IF (all from Novus Biologicals), rabbit anti–Aurora A at 1:1000 for IF, rabbit anti–phospho T288 Aurora A at 1:400 for IF, rabbit anti-HURP at 1:500 for IF, and mouse anti-Tacc3 at 1:1000 for IF (all from Abcam). For Western blot studies, rabbit anti–Aurora A was used at 1:1000 (BioLegend). When necessary, GFP-fusion protein signals were enhanced in IF with GFP-booster 1:200 (ChromoTek) or sheep anti-GFP antibody at 1:200 (BD Biosciences).

Secondary antibodies were highly cross-subtracted Alexa Fluor 488–, 555–, 594–, and 647–conjugated anti-mouse, -human, -rabbit, -sheep, and -rat and used at 1:500 or 1:200 (Life Technologies) for IF. Cross-subtracted DyLight 488– and Cy3-conjugated donkey anti-rat and anti-mouse immunoglobulin G (IgG; Jackson ImmunoResearch) were used at 1:500 for IF. DAPI was used at 2 μg/ml. For Western blotting, primary antibodies were detected with horseradish peroxidase–conjugated secondaries diluted 1:5000 (Promega) and developed with ECL (GE Healthcare) or IR-conjugated secondaries (IRDye800, Rockland Immunochemicals; Alexa Fluor 680, Life Technologies) and visualized on a LI-COR Odyssey (LI-COR Biosciences).

All images were stored in OMERO, and figures were generated using OMERO.figure, Fiji, or Photoshop (Adobe).

Immunoblotting and immunoprecipitation

G2/M-arrested cells were obtained by mitotic shake off. Mitotic enriched extracts or whole-cell extracts were prepared by lysing cells in 10 mM Tris-HCl, pH 7.5, 500 mM NaCl, 0.5 mM EDTA, 0.5% NP-40, and EDTA-free complete protease inhibitor mix (Roche). When phosphoproteins were to be analyzed, 1× Phospho STOP (Roche) was added to the lysis buffer.

For immunoprecipitation, lysates were cleared by a prespin at 20,000 × g for 5 min at 4°C, preequilibrated in 20 mM 4-(2-hydroxyethyl)-1-piperazineethanesulfonic acid, pH 7.9, 0.5 mM dithiothreitol and 20% glycerol, and incubated for 16 h at 4°C with anti-ALADIN, anti-GFP, or control IgG (Sigma-Aldrich), followed by 2-h incubation with rotation with protein G–Sepharose beads (Pierce) at 4°C. Beads were washed three times with cold PBS buffer, and bound proteins were eluted in 2× LDS-sample buffer (NuPAGE; Life Technologies).

Immunoprecipitated proteins or cell extracts were separated on NuPAGE 4–12% Bis-Tris Gels (Life Technologies) and then transferred to nitrocellulose membranes, and Western analysis was performed as described (Griffis *et al.*, 2007).

Statistical analysis

Data obtained from Omero and Fiji were imported into sigma-plot software, which was used to generate box-and-whisker and polar plots. In box-and-whisker plots, the middle line shows the median value; the bottom and top of the box show the lower and upper quartiles; whiskers extend to 10th and 90th percentiles; and all outliers are shown. To determine statistical significance between two treatments, we used Student's *t* test, and to evaluate three or more data sets, we used one-way analysis of variance (significance is reported on each figure).

REFERENCES

Allan C, Burel JM, Moore J, Blackburn C, Linkert M, Loynton S, Macdonald D, Moore WJ, Neves C, Patterson A, *et al.* (2012). OMERO: flexible, model-driven data management for experimental biology. Nat Methods 9, 245–253.

Arnaoutov A., Dasso M (2003). The Ran GTPase regulates kinetochore function. Dev Cell 5, 99–111.

Asteriti IA, Di Cesare E, De Mattia F, Hilsenstein V, Neumann B, Cundari E, Lavia P, Guarguaglini G (2014). The Aurora-A inhibitor MLN8237 affects multiple mitotic processes and induces dose-dependent mitotic abnormalities and aneuploidy. Oncotarget 5, 6229–6242.

Asteriti IA, Giubettini M, Lavia P, Guarguaglini G (2011). Aurora-A inactivation causes mitotic spindle pole fragmentation by unbalancing microtubule-generated forces. Mol Cancer 10, 131.

Babu JR, Jeganathan KB, Baker DJ, Wu X, Kang-Decker N, van Deursen JM (2003). Rae1 is an essential mitotic checkpoint regulator that cooperates with Bub3 to prevent chromosome missegregation. J Cell Biol 160, 341–353.

Bakhoum SF, Thompson SL, Manning AL, Compton DA (2009). Genome stability is ensured by temporal control of kinetochore-microtubule dynamics. Nat Cell Biol 11, 27–35.

Bayliss R, Sardon T, Vernos I, Conti E (2003). Structural basis of Aurora-A activation by TPX2 at the mitotic spindle. Mol Cell 12, 851–862.

Belgareh N, Rabut G, Bai SW, van Overbeek M, Beaudouin J, Daigle N, Zatsepina OV, Pasteau F, Labas V, Fromont-Racine M, *et al.* (2001). An evolutionarily conserved NPC subcomplex, which redistributes in part to kinetochores in mammalian cells. J Cell Biol 154, 1147–1160.

Bird AW, Hyman AA (2008). Building a spindle of the correct length in human cells requires the interaction between TPX2 and Aurora A. J Cell Biol 182, 289–300.

Blower MD, Nachury M, Heald R, Weis K (2005). A Rae1-containing ribonucleoprotein complex is required for mitotic spindle assembly. Cell 121, 223–234.

Boisvert FM, Ahmad Y, Gierlinski M, Charriere F, Lamont D, Scott M, Barton G, Lamond AI (2012). A quantitative spatial proteomics analysis of proteome turnover in human cells. Mol Cell Proteomics 11, M111.011429.

Bowman SK, Neumuller RA, Novatchkova M, Du Q, Knoblich JA (2006). The Drosophila NuMA Homolog Mud regulates spindle orientation in asymmetric cell division. Dev Cell 10, 731–742.

Chatel G, Fahrenkrog B (2011). Nucleoporins: leaving the nuclear pore complex for a successful mitosis. Cell Signal 23, 1555–1562.

Cheeseman LP, Booth DG, Hood FE, Prior IA, Royle SJ (2011). Aurora A kinase activity is required for localization of TACC3/ch-TOG/clathrin inter-microtubule bridges. Commun Integr Biol 4, 409–412.

Chen H, Mohan P, Jiang J, Nemirovsky O, He D, Fleisch MC, Niederacher D, Pilarski LM, Lim CJ, Maxwell CA (2014). Spatial regulation of Aurora A activity during mitotic spindle assembly requires RHAMM to correctly localize TPX2. Cell Cycle 13, 2248–2261.

Ciciarello M, Mangiacasale R, Lavia P (2007). Spatial control of mitosis by the GTPase Ran. Cell Mol Life Sci 64, 1891–1914.

Compton DA, Cleveland DW (1993). NuMA is required for the proper completion of mitosis. J Cell Biol 120, 947–957.

Conduit PT, Richens JH, Wainman A, Holder J, Vicente CC, Pratt MB, Dix CI, Novak ZA, Dobbie IM et al. (2014). A molecular mechanism of mitotic centrosome assembly in Drosophila. eLife 3, e03399.

Cronshaw JM, Krutchinsky AN, Zhang W, Chait BT, Matunis MJ (2002). Proteomic analysis of the mammalian nuclear pore complex. J Cell Biol 158, 915–927.

Cronshaw JM, Matunis MJ (2003). The nuclear pore complex protein ALADIN is mislocalized in triple A syndrome. Proc Natl Acad Sci USA 100, 5823–5827.

Cross MK, Powers MA (2011). Nup98 regulates bipolar spindle assembly through association with microtubules and opposition of MCAK. Mol Biol Cell 22, 661–672.

Dodson CA, Bayliss R (2012). Activation of Aurora-A kinase by protein partner binding and phosphorylation are independent and synergistic. J Biol Chem 287, 1150–1157.

Dodson CA, Yeoh S, Haq T, Bayliss R (2013). A kinetic test characterizes kinase intramolecular and intermolecular autophosphorylation mechanisms. Sci Signal 6, ra54.

Eyers PA, Maller JL (2003). Regulating the regulators: Aurora A activation and mitosis. Cell Cycle 2, 287–289.

Eyers PA, Maller JL (2004). Regulation of Xenopus Aurora A activation by TPX2. J Biol Chem 279, 9008–9015.

Goodman B, Channels W, Qiu M, Iglesias P, Yang G, Zheng Y (2010). Lamin B counteracts the kinesin Eg5 to restrain spindle pole separation during spindle assembly. J Biol Chem 285, 35238–35244.

Goodwin SS, Vale RD (2010). Patronin regulates the microtubule network by protecting microtubule minus ends. Cell 143, 263–274.

Goshima G, Wollman R, Goodwin SS, Zhang N, Scholey JM, Vale RD, Stuurman N (2007). Genes required for mitotic spindle assembly in Drosophila S2 cells. Science 316, 417–421.

Griffis ER, Stuurman N, Vale RD (2007). Spindly, a novel protein essential for silencing the spindle assembly checkpoint, recruits dynein to the kinetochore. J Cell Biol 177, 1005–1015.

Handschug K, Sperling S, Yoon SJ, Hennig S, Clark AJ, Huebner A (2001). Triple A syndrome is caused by mutations in AAAS, a new WD-repeat protein gene. Hum Mol Genet 10, 283–290.

Harel A, Chan RC, Lachish-Zalait A, Zimmerman E, Elbaum M, Forbes DJ (2003). Importin beta negatively regulates nuclear membrane fusion and nuclear pore complex assembly. Mol Biol Cell 14, 4387–4396.

Hirano M, Furiya Y, Asai H, Yasui A, Ueno S (2006). ALADINI482S causes selective failure of nuclear protein import and hypersensitivity to oxidative stress in triple A syndrome. Proc Natl Acad Sci USA 103, 2298–2303.

Hirota T, Kunitoku N, Sasayama T, Marumoto T, Zhang D, Nitta M, Hatakeyama K, Saya H (2003). Aurora-A and an interacting activator, the LIM protein Ajuba, are required for mitotic commitment in human cells. Cell 114, 585–598.

Hochegger H, Hegarat N, Pereira-Leal JB (2013). Aurora at the pole and equator: overlapping functions of Aurora kinases in the mitotic spindle. Open Biol 3, 120185.

Huebner A, Mann P, Rohde E, Kaindl AM, Witt M, Verkade P, Jakubiczka S, Menschikowski M, Stoltenburg-Didinger G, Koehler K (2006). Mice lacking the nuclear pore complex protein ALADIN show female infertility but fail to develop a phenotype resembling human triple A syndrome. Mol Cell Biol 26, 1879–1887.

Hutterer A, Berdnik D, Wirtz-Peitz F, Zigman M, Schleiffer A, Knoblich JA (2006). Mitotic activation of the kinase Aurora-A requires its binding partner Bora. Dev Cell 11, 147–157.

Itoh G, Sugino S, Ikeda M, Mizuguchi M, Kanno S, Amin MA, Iemura K, Yasui A, Hirota T, Tanaka K (2013). Nucleoporin Nup188 is required for chromosome alignment in mitosis. Cancer Sci 104, 871–879.

Jang CY, Coppinger JA, Seki A, Yates JR 3rd, Fang G (2009). Plk1 and Aurora A regulate the depolymerase activity and the cellular localization of Kif2a. J Cell Sci 122, 1334–1341.

Jeganathan KB, Malureanu L, van Deursen JM (2005). The Rae1-Nup98 complex prevents aneuploidy by inhibiting securin degradation. Nature 438, 1036–1039.

Joseph J, Liu ST, Jablonski SA, Yen TJ, Dasso M (2004). The RanGAP1-RanBP2 complex is essential for microtubule-kinetochore interactions in vivo. Curr Biol 14, 611–617.

Joukov V (2011). Aurora kinases and spindle assembly: variations on a common theme? Cell Cycle 10, 895–903.

Joukov V, De Nicolo A, Rodriguez A, Walter JC, Livingston DM (2010). Centrosomal protein of 192 kDa (Cep192) promotes centrosome-driven spindle assembly by engaging in organelle-specific Aurora A activation. Proc Natl Acad Sci USA 107, 21022–21027.

Joukov V, Walter JC, De Nicolo A (2014). The Cep192-organized aurora A-Plk1 cascade is essential for centrosome cycle and bipolar spindle assembly. Mol Cell 55, 578–591.

Kalab P, Heald R (2008). The RanGTP gradient—a GPS for the mitotic spindle. J Cell Sci 121, 1577–1586.

Kettenbach AN, Schweppe DK, Faherty BK, Pechenick D, Pletnev AA, Gerber SA (2011). Quantitative phosphoproteomics identifies substrates and functional modules of Aurora and Polo-like kinase activities in mitotic cells. Sci Signal 4, rs5.

Kind B, Koehler K, Krumbholz M, Landgraf D, Huebner A (2010). Intracellular ROS level is increased in fibroblasts of triple A syndrome patients. J Mol Med (Berl) 88, 1233–1242.

Kind B, Koehler K, Lorenz M, Huebner A (2009). The nuclear pore complex protein ALADIN is anchored via NDC1 but not via POM121 and GP210 in the nuclear envelope. Biochem Biophys Res Commun 390, 205–210.

King JM, Nicklas RB (2000). Tension on chromosomes increases the number of kinetochore microtubules but only within limits. J Cell Sci 113, 3815–3823.

Kiriyama T, Hirano M, Asai H, Ikeda M, Furiya Y, Ueno S (2008). Restoration of nuclear-import failure caused by triple A syndrome and oxidative stress. Biochem Biophys Res Commun 374, 631–634.

Klein UR, Haindl M, Nigg EA, Muller S (2009). RanBP2 and SENP3 function in a mitotic SUMO2/3 conjugation-deconjugation cycle on Borealin. Mol Biol Cell 20, 410–418.

Krumbholz M, Koehler K, Huebner A (2006). Cellular localization of 17 natural mutant variants of ALADIN protein in triple A syndrome—shedding light on an unexpected splice mutation. Biochem Cell Biol 84, 243–249.

Lee SH, Sterling H, Burlingame A, McCormick F (2008). Tpr directly binds to Mad1 and Mad2 and is important for the Mad1-Mad2-mediated mitotic spindle checkpoint. Genes Dev 22, 2926–2931.

Lince-Faria M, Maffini S, Orr B, Ding Y, Claudia F, Sunkel CE, Tavares A, Johansen J, Johansen KM, Maiato H (2009). Spatiotemporal control of mitosis by the conserved spindle matrix protein Megator. J Cell Biol 184, 647–657.

Lioutas A, Vernos I (2014). Aurora A: working from dawn to dusk in mitosis. Cell Cycle 13, 499–500.

Littlepage LE, Wu H, Andresson T, Deanehan JK, Amundadottir LT, Ruderman JV (2002). Identification of phosphorylated residues that affect the activity of the mitotic kinase Aurora-A. Proc Natl Acad Sci USA 99, 15440–15445.

Loiodice I, Alves A, Rabut G, Van Overbeek M, Ellenberg J, Sibarita JB, Doye V (2004). The entire Nup107-160 complex, including three new members, is targeted as one entity to kinetochores in mitosis. Mol Biol Cell 15, 3333–3344.

Merdes A, Heald R, Samejima K, Earnshaw WC, Cleveland DW (2000). Formation of spindle poles by dynein/dynactin-dependent transport of NuMA. J Cell Biol 149, 851–862.

Merdes A, Ramyar K, Vechio JD, Cleveland DW (1996). A complex of NuMA and cytoplasmic dynein is essential for mitotic spindle assembly. Cell 87, 447–458.

Meunier S, Vernos I (2011). K-fibre minus ends are stabilized by a RanGTP-dependent mechanism essential for functional spindle assembly. Nat Cell Biol 13, 1406–1414.

Mishra RK, Chakraborty P, Arnaoutov A, Fontoura BM, Dasso M (2010). The Nup107-160 complex and gamma-TuRC regulate microtubule polymerization at kinetochores. Nat Cell Biol 12, 164–169.

Olsen JV, Vermeulen M, Santamaria A, Kumar C, Miller ML, Jensen LJ, Gnad F, Cox J, Jensen TS, Nigg EA, *et al.* (2010). Quantitative phosphoproteomics reveals widespread full phosphorylation site occupancy during mitosis. Sci Signal 3, ra3.

Orjalo AV, Arnaoutov A, Shen Z, Boyarchuk Y, Zeitlin SG, Fontoura B, Briggs S, Dasso M, Forbes DJ (2006). The Nup107-160 nucleoporin complex is required for correct bipolar spindle assembly. Mol Biol Cell 17, 3806–3818.

Otsu N (1979). Threshold selection method from gray-level histograms. IEEE Trans Syst Man Cybernet 9, 62–66.

Pinyol R, Scrofani J, Vernos I (2013). The role of NEDD1 phosphorylation by Aurora A in chromosomal microtubule nucleation and spindle function. Curr Biol 23, 143–149.

Platani M, Santarella-Mellwig R, Posch M, Walczak R, Swedlow JR, Mattaj IW (2009). The Nup107-160 nucleoporin complex promotes mitotic events via control of the localization state of the chromosome passenger complex. Mol Biol Cell 20, 5260–5275.

Poser I, Sarov M, Hutchins JR, Heriche JK, Toyoda Y, Pozniakovsky A, Weigl D, Nitzsche A, Hegemann B, Bird AW, *et al.* (2008). BAC TransgeneOmics: a high-throughput method for exploration of protein function in mammals. Nat Methods 5, 409–415.

Prasad R, Metherell LA, Clark AJ, Storr HL (2013). Deficiency of ALADIN impairs redox homeostasis in human adrenal cells and inhibits steroidogenesis. Endocrinology 154, 3209–3218.

Prunuske AJ, Liu J, Elgort S, Joseph J, Dasso M, Ullman KS (2006). Nuclear envelope breakdown is coordinated by both Nup358/RanBP2 and Nup153, two nucleoporins with zinc finger modules. Mol Biol Cell 17, 760–769.

Rasala BA, Ramos C, Harel A, Forbes DJ (2008). Capture of AT-rich chromatin by ELYS recruits POM121 and NDC1 to initiate nuclear pore assembly. Mol Biol Cell 19, 3982–3996.

Reboutier D, Troadec MB, Cremet JY, Fukasawa K, Prigent C (2012). Nucleophosmin/B23 activates Aurora A at the centrosome through phosphorylation of serine 89. J Cell Biol 197, 19–26.

Rogers SL, Rogers GC (2008). Culture of Drosophila S2 cells and their use for RNAi-mediated loss-of-function studies and immunofluorescence microscopy. Nat Protoc 3, 606–611.

Rome P, Montembault E, Franck N, Pascal A, Glover DM, Giet R (2010). Aurora A contributes to p150(glued) phosphorylation and function during mitosis. J Cell Biol 189, 651–659.

Samora CP, McAinsh AD (2011). Photoactivatable-GFP-alpha-tubulin as a tool to study microtubule plus-end turnover in living human cells. Methods Mol Biol 777, 223–233.

Sardon T, Pache RA, Stein A, Molina H, Vernos I, Aloy P (2010). Uncovering new substrates for Aurora A kinase. EMBO Rep 11, 977–984.

Satinover DL, Leach CA, Stukenberg PT, Brautigan DL (2004). Activation of Aurora-A kinase by protein phosphatase inhibitor-2, a bifunctional signaling protein. Proc Natl Acad Sci USA 101, 8625–8630.

Schweizer N, Weiss M, Maiato H (2014). The dynamic spindle matrix. Curr Opin Cell Biol 28, 1–7.

Sdelci S, Schutz M, Pinyol R, Bertran MT, Regue L, Caelles C, Vernos I, Roig J (2012). Nek9 phosphorylation of NEDD1/GCP-WD contributes to Plk1 control of gamma-tubulin recruitment to the mitotic centrosome. Curr Biol 22, 1516–1523.

Silk AD, Holland AJ, Cleveland DW (2009). Requirements for NuMA in maintenance and establishment of mammalian spindle poles. J Cell Biol 184, 677–690.

Sillje HH, Nagel S, Korner R, Nigg EA (2006). HURP is a Ran-importin beta-regulated protein that stabilizes kinetochore microtubules in the vicinity of chromosomes. Curr Biol 16, 731–742.

Silva VC, Cassimeris L (2013). Stathmin and microtubules regulate mitotic entry in HeLa cells by controlling activation of both Aurora kinase A and Plk1. Mol Biol Cell 24, 3819–3831.

Silverman-Gavrila RV, Wilde A (2006). Ran is required before metaphase for spindle assembly and chromosome alignment and after metaphase for chromosome segregation and spindle midbody organization. Mol Biol Cell 17, 2069–2080.

Storr HL, Kind B, Parfitt DA, Chapple JP, Lorenz M, Koehler K, Huebner A, Clark AJ (2009). Deficiency of ferritin heavy-chain nuclear import in triple a syndrome implies nuclear oxidative damage as the primary disease mechanism. Mol Endocrinol 23, 2086–2094.

Toughiri R, Li X, Du Q, Bieberich CJ (2013). Phosphorylation of NuMA by Aurora-A kinase in PC-3 prostate cancer cells affects proliferation, survival, and interphase NuMA localization. J Cell Biochem 114, 823–830.

Tsai CY, Ngo B, Tapadia A, Hsu PH, Wu G, Lee WH (2011). Aurora-A phosphorylates Augmin complex component Hice1 protein at an N-terminal serine/threonine cluster to modulate its microtubule binding activity during spindle assembly. J Biol Chem 286, 30097–30106.

Tsai MY, Wang S, Heidinger JM, Shumaker DK, Adam SA, Goldman RD, Zheng Y (2006). A mitotic lamin B matrix induced by RanGTP required for spindle assembly. Science 311, 1887–1893.

Tsai MY, Wiese C, Cao K, Martin O, Donovan P, Ruderman J, Prigent C, Zheng Y (2003). A Ran signalling pathway mediated by the mitotic kinase Aurora A in spindle assembly. Nat Cell Biol 5, 242–248.

Wang LH, Yan M, Xu DZ, Cao JX, Zhu XF, Zeng YX, Liu Q (2008). Requirement of Aurora-A kinase in astral microtubule polymerization and spindle microtubule flux. Cell Cycle 7, 1104–1111.

Wong J, Lerrigo R, Jang CY, Fang G (2008). Aurora A regulates the activity of HURP by controlling the accessibility of its microtubule-binding domain. Mol Biol Cell 19, 2083–2091.

Xu S, Powers MA (2010). Nup98-homeodomain fusions interact with endogenous Nup98 during interphase and localize to kinetochores and chromosome arms during mitosis. Mol Biol Cell 21, 1585–1596.

Zeng K, Bastos RN, Barr FA, Gruneberg U (2010). Protein phosphatase 6 regulates mitotic spindle formation by controlling the T-loop phosphorylation state of Aurora A bound to its activator TPX2. J Cell Biol 191, 1315–1332.

Zhang X, Ems-McClung SC, Walczak CE (2008). Aurora A phosphorylates MCAK to control ran-dependent spindle bipolarity. Mol Biol Cell 19, 2752–2765.

Zhao ZS, Lim JP, Ng YW, Lim L, Manser E (2005). The GIT-associated kinase PAK targets to the centrosome and regulates Aurora-A. Mol Cell 20, 237–249.

Zheng Y (2010). A membranous spindle matrix orchestrates cell division. Nat Rev Mol Cell Biol 11, 529–535.

Zorba A, Buosi V, Kutter S, Kern N, Pontiggia F, Cho YJ, Kern D (2014). Molecular mechanism of Aurora A kinase autophosphorylation and its allosteric activation by TPX2. eLife 3, e02667.